Unusual architecture of the p7 channel from hepatitis C virus

Published in final edited form as:
Nature. 2013 June 27; 498(7455): . doi:10.1038/nature12283.

Unusual architecture of the p7 channel from hepatitis C virus

Bo OuYang[1,2,3], **Shiqi Xie**[4], **Marcelo J. Berardi**[1], **Xinhao Zhao**[4], **Jyoti Dev**[1], **Wenjing Yu**[4], **Bing Sun**[4,5], and **James J. Chou**[1,2,3]

[1]Department of Biological Chemistry and Molecular Pharmacology, Harvard Medical School, Boston, Massachusetts 02115, USA

[2]State Key Laboratory of Molecular Biology, Shanghai Institute of Biochemistry and Cell Biology, Chinese Academy of Sciences, Shanghai 200031, China

[3]National Center for Protein Science, Shanghai Institute of Biochemistry and Cell Biology, Chinese Academy of Sciences, Shanghai 200031, China

[4]Molecular Virus Unit, Key laboratory of Molecular Virology and Immunology, Institut Pasteur of Shanghai, Shanghai Institutes for Biological Sciences, Chinese Academy of Sciences, Shanghai 200025, China

[5]State Key Laboratory of Cell Biology, Shanghai Institute of Biochemistry and Cell Biology, Chinese Academy of Sciences, Shanghai 200031, China

Abstract

The Hepatitis C virus (HCV) has developed a small membrane protein, p7, which remarkably can self-assemble into a large channel complex that selectively conducts cations[1-4]. We are curious as to what structural solution has the viroporin adopted to afford selective cation conduction because p7 has no homology with any of the known prokaryotic or eukaryotic channel proteins. The p7 activity can be inhibited by amantadine and rimantadine[2,5], which also happen to be potent blockers of the influenza M2 channel[6] and licensed drugs against influenza infections[7]. The adamantane derivatives were subjects of HCV clinical trials[8], but large variation in drug efficacy among the various HCV genotypes has been difficult to explain without detailed molecular structures. Here, we determined the structures of this HCV viroporin as well as its drug-binding site using the latest nuclear magnetic resonance (NMR) technologies. The structure exhibits an unusual mode of hexameric assembly, where the individual p7 monomers, *i*, not only interact with their immediate neighbors, but also reach farther to associate with the *i*+2 and *i*+3 monomers, forming a sophisticated, funnel-like architecture. The structure also alludes to a mechanism of cation selection: an asparagine/histidine ring that constricts the narrow end of the funnel serves as a broad cation selectivity filter while an arginine/lysine ring that defines the wide end of the funnel may selectively allow cation diffusion into the channel. Our functional investigation using whole-cell channel recording showed that these residues are indeed critical for channel activity. NMR measurements of the channel-drug complex revealed six equivalent hydrophobic pockets between the peripheral and pore-forming helices to which amantadine or rimantadine binds, and compound binding specifically to this position may allosterically inhibit cation conduction by preventing the channel from opening. Our data provide molecular explanation for p7-mediated cation conductance and its inhibition by adamantane derivatives.

Correspondence and requests for materials should be addressed to J.J.C. (chou@cmcd.hms.harvard.edu) and B.S. (bsun@sibs.ac.cn).

Author Contributions B.O. and J.J.C. conceived of the study; B.O. prepared samples; M.J.B. performed EM analysis; J.D. and B.O. performed NMR titration; B.O. and J.J.C. collected and analyzed NMR data and determined the structure; S.X., X.Z., W.Y., B.S. designed and performed functional experiments; J.J.C. wrote the paper and all authors contributed to editing of the manuscript.

The structure will be deposited in the Protein Data Bank under the accession number 2M6X.

Many viruses have developed integral membrane proteins to transport ions and other molecules across the membrane barrier to aid various steps of viral entry and maturation[9,10]. These membrane structures, known as viroporins, usually adopt minimalist architectures that are significantly different from those of bacterial or eukaryotic ion channels. Therefore, understanding the structural basis of how viroporins function broadens our knowledge of channels and transporters while generating new opportunities for therapeutic intervention.

The viroporin formed by the HCV p7 protein has been sought after as potential anti-HCV drug target[5,11]. p7 is a 63-residue membrane protein that oligomerizes to form ion channels with cation selectivity, for Ca^{2+} over K^+ and Na^+[2,3,12,13], and more recent studies also reported p7-mediated H^+ intracellular conductance[14]. The p7 channel is required for viral replication1[5]; it has been shown to facilitate efficient assembly and release of infectious virions[16,17], though the precise mechanism of these functions remains unclear. The channel activity can be inhibited by adamantane and long alkylchain iminosugar derivatives and hexamethylene amiloride *in vitro*, with varying reported efficacies[2,3,12,13]. In addition to ion conduction, p7 has been shown to specifically interact with the non-structural HCV protein NS2, suggesting that its channel activity could be regulated[18,19].

There is not yet a detailed structure of the p7 channel, though a number of pioneering NMR studies showed that the p7 monomer has three helical segments: two in the N-terminal half of the sequence and one near the C-terminus[12,20]. A single-particle electron microscopy (EM) study obtained a 16 Å resolution electron density map of the p7 oligomer using the random conical tilting approach[4]. The map shows that the p7 channel is a 42 kDa hexamer and adopts a flower-like shape that does not resemble any of the known ion channel structures in the database.

How does the small p7 polypeptide assemble into what appears to be a complex channel structure? Has the viroporin adopted novel structural elements for cation selectivity and channel gating? Amantadine or rimantadine blocks the influenza M2 channel by binding to the small pore formed by four transmembrane helices[21-23], but the pore of the p7 hexamer is expected to be much bigger and it is thus unclear how would these small molecules fit. We sought to address these important questions by determining detailed structures of the p7 hexamer and its drug-binding site.

We systematically tested p7 amino acid sequences from various HCV genotypes and found that the sequence from genotype 5a (EUH1480 strain) generated samples that were sufficiently soluble for structure determination (Supplementary Fig. 1). This p7 construct, designated here as p7(5a), could be efficiently reconstituted in dodecylphosphocholine (DPC) micelles at near physiological pH and generated high quality NMR spectra (Supplementary Fig. 2). Negative-stain EM of the DPC-reconstituted p7(5a) in NMR buffer showed hexameric, flower-shaped particles that are similar to those in the electron micrographs of the p7 (JFH-1 strain, genotype 2a) hexamer in dihexanoyl-phosphatidyl-choline (DHPC) micelles used earlier for single-particle reconstruction[4] (Supplementary Fig. 3). Moreover, isothermal titration calorimetry and NMR chemical shift perturbation analyses of p7(5a)-rimantadine interaction showed that the drug binds specifically to the reconstituted protein with a binding constant (K_d) from 50-100 μM at 3 mM detergent concentration (Supplementary Fig. 4&5). The above results together indicate that the p7(5a) polypeptides reconstituted in DPC micelles form structurally relevant hexamers.

Structure determination of the p7(5a) hexamer by NMR employed approach taken earlier for oligomeric membrane proteins[24-26], which involves 1) determination of local structures of the monomers and 2) assembly of the oligomer with intermonomer distance restraints and orientation constraints. The NMR-derived restraints define an ensemble of structures with

backbone r.m.s. deviation of 0.74 Å (Fig. 1a). Each monomer consists of an N-terminal helix (H1) from residues 5-16, a middle helical segment (H2), with a kink at Gly34, from residues 20-41, and a C-terminal helix (H3) from residues 48-58. These secondary structures are consistent with earlier NMR studies of p7 monomers in DHPC detergent and organic solvent[12,20]. There are no intramonomer contacts (Fig. 1a). The monomers are intertwined to form a tightly packed channel, where H1 and H2 form the channel interior and H3 is lipid-facing and packs against H2 of the *i*+2 and H1 of the *i*+3 monomer (Fig. 1a&b). The intermonomer association between H3 and H2 appears to be stabilized by interaction involving conserved residues such as Trp30, Tyr42, and Leu52, and the contacts between H3 and H1 are mostly between the alanine rich region of H1 (residues 10-15) and Ala61 and Ala63 of H3 (Fig. 1c). The overall structure of the p7(5a) hexamer has a flower-like shape that agrees with the EM map (EM database ID:1661), fitting to the map with a correlation coefficient of 0.94 (Fig. 1d).

The channel cavity has a funnel profile that resembles a champagne flute and is largely hydrophilic (Fig. 2a). The H2 helices form the wide cylindrical region (internal diameter, I.D. ~12 Å) by packing with each other at large angles (angle between adjacent helices ~ -47°), and the H1 helices assemble at smaller packing angles (~ -34°) to form the narrow conical region of the funnel (smallest I.D. at 6.8 Å). Residues 17-19 constitute the flexible joint between H1 and H2; their NMR resonances are significantly broader than other regions of the protein, suggesting the presence of conformational exchange.

The channel architecture described above represents a novel topology and exemplifies how HCV has optimized the short p7 polypeptide to achieve a rather complex channel structure. What are then the elements for cation conduction and gating? An in-depth examination of the channel interior found two strongly conserved polar residues with salient structural features (Fig. 2b). One is Asn9, which forms a ring of carboxamide that constricts the conical region of the channel (Fig. 2c). Residue 9 is asparagine in all strains except being substituted with histidine in genotype 2 viruses. Both asparagines and histidines have affinity for monovalent and divalent cations. We hypothesize that the Asn9 ring serves as a broad selectivity filter that dehydrates cations, allowing them to pass the hydrophobic ring formed by Ile6. The Ile6 ring defines the narrowest point of the channel and likely serves as a hydrophobic gate. Another feature is the Arg35 ring that defines the wider, C-terminal end of the channel (Fig. 2b). Placement of a positively charged ring on the other end of the pore was incomprehensible to us initially because it can repel cations. But the recent structure of an Orai Ca^{2+} channel also revealed a stretch of basic residues in the ion conducting pore[27]. We hypothesize that one of the Arg35 roles is to bind and obstruct anions at the pore entrance while allowing cations to diffuse into the pore. In this model, cation conduction is unidirectional from the C- to N-terminal end of the channel.

To test the above hypotheses, we established an assay that uses the two-electrode voltage-clamp technique to record p7-mediated current in *Xenopus* oocytes (METHODS). Due to the poor stability of oocytes that overexpress p7(5a), p7 (JFH-1 strain, genotype 2a) was used instead for these experiments. As expected of the proposed role of residue 9 in selectively dehydrating cations, replacing His9 of p7(2a) with alanine caused ~70% reduction in channel conductance at +80 mV (Fig. 2d). The proposed role of Arg35 infers that placing negatively charged residues at the channel entrance would bind cations and hinder their diffusion into the pore, and indeed the R35D mutation also reduced conductance by ~70% (Fig. 2d).

We next investigated the mechanism of amantadine binding to the p7 channel using proteins that are ^{15}N-labeled and deuterated so that Nuclear Overhauser Enhancement (NOE) between the protein backbone amide protons and drug protons could be measured

unambiguously. At 10 mM amantadine (not corrected for drug partitioning to detergent micelles), the ^{15}N-edited NOESY spectrum showed NOE crosspeaks between the adamantane protons and the amide protons of Val26, Leu55, Leu56, and Arg57 (Fig. 3a). We then identified contacts between the drug and protein sidechains using protein that is (^{1}H/^{13}C)-labeled at the methyl positions of alanines, valines and leucines but is otherwise deuterated. In this case, the ^{13}C-edited NOESY showed several methyl-drug NOEs (Fig. 3b).

These NOEs were used to dock amantadine into the structure determined in the absence of drug. In doing so, we emphasize that the relevance of the p7-amantadine complex is confined to only the drug binding region because we do not know how and to what degree does drug binding alter the global conformation of the channel. The relatively poor stability of the protein-drug complex at the current stage of our study precludes full-scale structure determination. Nonetheless the available NMR data show that the drug adamantane binds to six equivalent hydrophobic pockets between the pore-forming and peripheral helices (Fig. 3c). The pocket consists of Leu52, Val53, and Leu56 from H3, and Phe20, Val25, and Val26 from H2. The amantadine amino group on average points to the channel lumen. The same NOESY spectrum as above recorded using a sample with 5 mM rimantadine indicates that rimantadine binds to the same pocket with the methyl and amino groups pointing to the lumen (Supplementary Fig. 6).

The binding site is overall consistent with mutational study showing that mutations in residues 50-55 significantly reduced drug sensitivity of the channel[28]. It is also consistent with a L20F mutation in genotype 1b virus originally identified in clinical trials that confers amantadine resistance[8,29]. In the p7(5a) structure, residue 20 is an integral part of the drug pocket and is in direct contact with the drug adamantane. Therefore, replacing Leu20 in p7(1b) with phenylalanine is expected to reduce hydrophobic interaction with the drug. Elucidation of previous functional data in the context of the structure suggests that the binding site shown in Fig. 3c is relevant to drug inhibition and that interactions between the drug adamantane and protein hydrophobic residues are critical for inhibition. Variations in the hydrophobicity of the binding pocket among the p7 variants (Supplementary Fig. 7) thus explain the large differences in drug efficacies observed between different HCV genotypes.

We have learnt from KcsA and other channels that a gated ion channel generally adopts two essential features: pore elements that provide ion selectivity and gating mechanism that can transiently open the channel to allow ion permeation. By virtue of being a funnel, the p7 structure suggests that the tip of the funnel represented by the Ile6 and Asn9 rings is the key region for channel gating (Fig. 4). The role of the Asn9 ring is to provide ion selectivity by recruiting and dehydrating cations near the funnel exit, whereas the Ile6 ring is a hydrophobic constriction that would prevent water from freely passing through. Channel activation may involve reorientation of the H1 helices that widens the funnel tip, analogous to the dynamic C-terminal helix of KcsA[30], and such structural rearrangement can be afforded by the flexible hinge between H1 and H2, the intervening loop between H2 and H3, and the C-terminal tail that “latches” onto H1. We thus propose that binding of adamantane derivatives inhibit channel activity by restricting the structural rearrangement. Our NMR titration data (Supplementary Fig. 5c) is consistent with this proposal, which showed that in the absence of rimantadine, the Ile6 methyl resonance is split into an intense and weak peak, possibly corresponding to the open and closed state, respectively, and that increasing the drug concentration shifted the equilibrium that made the weak peak stronger. Although rigorous testing of the model is needed, the preliminary observation suggests the existence of multiple states of the p7 channel.

METHODS

Sample Preparation

The amino acid sequence of p7 from genotype 5a was slightly modified to allow for efficient reconstitution and protein sample stability. In this sequence, Thr1 is replaced with Gly, Ala12 is replaced with Ser, and the three cysteines at positions 2, 27, and 44 are replaced with Ala, Thr, and Ser, respectively (Supplementary Fig. 1). The p7(5a) construct was cloned, expressed and purified as previously described[1,2]. Briefly, the protein was expressed as a fusion to His9–trpLE that formed inclusion bodies. The peptide was released from the fusion protein by CNBr digestion and subsequently separated on a Proto-18C column by reverse-phase chromatography (more details given in Supplementary Methods). The lyophilized peptide was then dissolved in 6 M guanidine and DPC and refolded by dialysis against the NMR buffer. A typical NMR sample contains 0.8 mM protein (monomer concentration), 200 mM DPC, and 25 mM MES (pH 6.5).

Assignment of NMR resonances

All NMR experiments were conducted at 30 °C on Bruker spectrometers equipped with cryogenic probes. Sequence specific assignment of backbone chemical shifts was accomplished using three pairs of triple resonance experiments, recorded using a $^{15}N/^{13}C/^{2}H$ labeled sample. The triple resonance experiments were relaxation optimized (TROSY)[3], including HNCA, HN(CO)CA, HNCACB, HN(CO)CACB, HN(CA)CO, and HNCO[4]. Protein sidechain aliphatic and aromatic resonances were assigned using a combination of NOESYs including ^{15}N-edited NOESY-TROSY (60 ms NOE mixing time, τ_{NOE}) and ^{13}C-edited NOESY-HSQCs (τ_{NOE}=100 ms). Specific stereo assignment of the methyl groups of valines and leucines were obtained from a constant-time ^{1}H-^{13}C HSQC spectrum recorded using a 15% ^{13}C-labeled sample[5].

Assignment of local NOEs for determining the secondary structures

The same ^{15}N-edited NOESY-TROSY and ^{13}C-edited NOESY-HSQC above with short τ_{NOE} were used to assign local NOEs. Combining the NOE restraints with chemical shifts, we could very precisely define the helical and loop regions of the individual monomers.

Measurement of residual dipolar coupling (RDC) constants

The backbone ^{1}H-^{15}N RDCs were measured using a modified approach[6] of the strain-induced alignment in a gel method[7,8]. In this experiment the p7(5a) channel in DPC micelles was soaked into a cylindrically shaped polyacrylamide gel (4.5%), initially of 6 mm diameter, which was subsequently radially compressed to fit within the 4.2 mm inner diameter of an open-ended NMR tube. The ^{1}H-^{15}N RDCs were obtained from $^{1}J_{NH}/2$ and $(^{1}J_{NH}+^{1}D_{NH})/2$, which were measured by interleaving a regular gradient-enhanced HSQC and a gradient-selected TROSY[9]. The largest ^{1}H-^{15}N RDC measured is 33.5 Hz.

Assignment of intermonomer NOEs

Intermonomer NOEs between protein backbone amide and sidechain methyl protons was assigned using a sample that was reconstituted with a 1:1 mixture of ^{15}N-, ^{2}H-labeled p7(5a) peptide and ^{13}C-labeled peptide. Recording a ^{15}N-edited NOESY-TROSY (τ_{NOE}=300 ms) on a 900 MHz spectrometer with this sample allowed exclusive detection of NOE crosspeaks between the ^{15}N-attached protons of one monomer and the ^{13}C-attached protons of other monomers. The intermonomer NOEs between the neighboring H1 helices and neighboring H2 helices effectively defined the central cavity formed by these helices. The initial structural solution of the pore assembly then allowed us to assign complementary and self-consistent intermonomer NOEs between the aliphatic and aromatic protons in a pair

of ^{15}N-edited NOESY-TROSY and ^{13}C-edited NOESY-HSQC recorded using a ^{15}N-, ^{13}C-labeled sample. These spectra were recorded with τ_{NOE} of 120 ms and 150 ms, respectively.

The packing of H1 and H2 helices between the adjacent monomers and RDC-derived orientation constraints together positioned the H3 helix of monomer *i* to be in contact with H2 of the *i*+2 and H1 of the *i*+3 monomers, and this conformation was confirmed by the unambiguous amide-methyl NOEs between H3 and H1/H2. The conformation as defined by the intermonomer NOEs was subject to numerous rounds of self-consistency test with the NOE crosspeaks in the ^{13}C-edited NOESY-HSQC spectrum to ensure that all NOEs are consistent with the structure. The overall distribution of intermonomer NOEs is illustrated in Supplementary Fig. 7.

Assignment of NOEs between protein and drug

We prepared a sample containing ^{15}N-, ^{2}H-labeled p7(5a), 10 mM amantadine (or 5 mM rimantadine), and perdeuterated DPC. The sample was used to record a ^{15}N-edited NOESY-TROSY (τ_{NOE}=300 ms) on a 900 MHz spectrometer. This experiment allowed exclusive detection of NOEs between the exchangeable amide protons and the drug protons. For assigning NOEs between the protein sidechain methyl protons and the drug protons, we prepared the ALV-labeled protein that is ^{1}H-, ^{13}C-labeled at the methyl positions of alanines, valines and leucines but is otherwise deuterated. The NOEs were measured using a ^{13}C-edited NOESY with diagonal suppression, i.e., interleaving two experiments: one with NOE mixing (300 ms) of the H_z magnetization (NOE crosspeaks) and the other with mixing of the H_zC_z magnetization (no NOE crosspeaks)[10]. Subtracting the two spectra mostly cancelled the strong methyl diagonal peaks (~0.8 ppm) and thereby unveiled the weak methyl-drug NOEs at ~1.7 ppm.

Structure calculation of the p7(5a) hexamer

Structures were calculated using the program XPLOR-NIH[11]. The monomer structures (mainly the secondary structures) were first calculated using intramonomer NOE-derived distance restraints, backbone dihedral restraints derived from chemical shifts using the TALOS program[12], and RDC restraints. A total of 10 monomer structures were calculated using a standard simulated annealing (SA) protocol. Six copies of the lowest-energy monomer structure were used to construct an initial model of the hexamer using intermonomer NOE restraints collected from the mixed-labeled sample for the H1 and H2 helical segments. For each intermonomer restraint between two adjacent monomers, six identical distance restraints were assigned respectively to all pairs of neighboring monomers to satisfy the condition of C6 rotational symmetry (as indicated by the EM data). The assembled hexamer was then subject to refinement against RDCs to accurately orient the three helical segments. Finally, using the SA protocol, the hexamer was refined against the complete set of NOE restraints (including intramonomer and intermonomer distance restraints), dihedral restraints, and RDC restraints. A total of 60 hexamer structures were calculated and 15 low energy structures were selected as the structural ensemble. Ramachandran plot statistics for the structure ensemble, calculated using PROCHECK[13], are as follows: most favored (96.6%), additionally allowed (2.8%), generously allowed (0.6%) and disallowed (0.0%).

Whole-cell channel recording assay for p7

The cRNA of p7(2a) variants were synthesized and injected into *Xenopus laevis* oocytes at ~15 ng per oocyte. After about 16-30 hours of expression, healthy oocytes were collected and subject to channel recording using the two-electrode voltage-clamp technique[14]. The oocytes were first bathed in standard ORi solution (90 mM NaCl, 2 mM KCl, 2 mM $CaCl_2$, and 5 mM MOPS, pH 7.4) before impaled with two microelectrodes. For recording p7-

mediated current, we used a voltage-clamp protocol consisting of rectangular voltage steps from −100 to +80 mV in 10 mV increments, applied from a holding voltage of −60 mV. Expression levels of the p7 variants in oocytes were examined by confocal microscopy using HA-tagged p7. More experimental details are described in Supplementary Methods.

Supplementary Material

Refer to Web version on PubMed Central for supplementary material.

Acknowledgments

We thank Remy Sounier for helping with making specific methyl labeled protein, Sven Brueschweiler for helping with ITC measurements, Gaëtan Bellot, Jianghong Min, and William Shih for providing DNA nanotube liquid crystal, and Kirill Oxenoid for helpful discussion. This work was supported by the National Key Project of 973 (2013CB530504) and National Science and Technology Major Project (2012ZX10002-007-003) (to B.S.) and NIH Grant GM094608 (to J.J.C.).

References

1. Moradpour D, Penin F, Rice CM. Replication of hepatitis C virus. Nat Rev Microbiol. 2007; 5:453–463. [PubMed: 17487147]
2. Griffin SD, et al. The p7 protein of hepatitis C virus forms an ion channel that is blocked by the antiviral drug, Amantadine. FEBS Lett. 2003; 535:34–38. [PubMed: 12560074]
3. Pavlovic D, et al. The hepatitis C virus p7 protein forms an ion channel that is inhibited by long-alkylchain iminosugar derivatives. Proc Natl Acad Sci U S A. 2003; 100:6104–6108. [PubMed: 12719519]
4. Luik P, et al. The 3-dimensional structure of a hepatitis C virus p7 ion channel by electron microscopy. Proc Natl Acad Sci U S A. 2009; 106:12712–12716. [PubMed: 19590017]
5. Griffin S, et al. Genotype-dependent sensitivity of hepatitis C virus to inhibitors of the p7 ion channel. Hepatology. 2008; 48:1779–1790. [PubMed: 18828153]
6. Wang C, Takeuchi K, Pinto LH, Lamb RA. Ion channel activity of influenza A virus M2 protein: characterization of the amantadine block. J Virol. 1993; 67:5585–5594. [PubMed: 7688826]
7. Davies WL, et al. Antiviral Activity of 1-Adamantanamine (Amantadine). Science. 1964; 144:862–863. [PubMed: 14151624]
8. Mihm U, et al. Amino acid variations in hepatitis C virus p7 and sensitivity to antiviral combination therapy with amantadine in chronic hepatitis C. Antivir Ther. 2006; 11:507–519. [PubMed: 16856625]
9. Fischer WB, Sansom MS. Viral ion channels: structure and function. Biochim Biophys Acta. 2002; 1561:27–45. [PubMed: 11988179]
10. Nieva JL, Madan V, Carrasco L. Viroporins: structure and biological functions. Nat Rev Microbiol. 2012; 10:563–574. [PubMed: 22751485]
11. Steinmann E, et al. Antiviral effects of amantadine and iminosugar derivatives against hepatitis C virus. Hepatology. 2007; 46:330–338. [PubMed: 17599777]
12. Montserret R, et al. NMR structure and ion channel activity of the p7 protein from hepatitis C virus. J Biol Chem. 2010; 285:31446–31461. [PubMed: 20667830]
13. Premkumar A, Wilson L, Ewart GD, Gage PW. Cation-selective ion channels formed by p7 of hepatitis C virus are blocked by hexamethylene amiloride. FEBS Lett. 2004; 557:99–103. [PubMed: 14741348]
14. Wozniak AL, et al. Intracellular proton conductance of the hepatitis C virus p7 protein and its contribution to infectious virus production. PLoS Pathog. 2010; 6:e1001087. [PubMed: 20824094]
15. Sakai A, et al. The p7 polypeptide of hepatitis C virus is critical for infectivity and contains functionally important genotype-specific sequences. Proc Natl Acad Sci U S A. 2003; 100:11646–11651. [PubMed: 14504405]

16. Jones CT, Murray CL, Eastman DK, Tassello J, Rice CM. Hepatitis C virus p7 and NS2 proteins are essential for production of infectious virus. J Virol. 2007; 81:8374–8383. [PubMed: 17537845]
17. Steinmann E, et al. Hepatitis C virus p7 protein is crucial for assembly and release of infectious virions. PLoS Pathog. 2007; 3:e103. [PubMed: 17658949]
18. Popescu CI, et al. NS2 protein of hepatitis C virus interacts with structural and non-structural proteins towards virus assembly. PLoS Pathog. 2011; 7:e1001278. [PubMed: 21347350]
19. Vieyres G, et al. Subcellular Localization and Function of an Epitope-Tagged p7 Viroporin in Hepatitis C Virus-Producing Cells. J Virol. 2013; 87:1664–1678. [PubMed: 23175364]
20. Cook GA, Opella SJ. Secondary structure, dynamics, and architecture of the p7 membrane protein from hepatitis C virus by NMR spectroscopy. Biochim Biophys Acta. 2011; 1808:1448–1453. [PubMed: 20727850]
21. Stouffer AL, et al. Structural basis for the function and inhibition of an influenza virus proton channel. Nature. 2008; 451:596–599. [PubMed: 18235504]
22. Cady SD, et al. Structure of the amantadine binding site of influenza M2 proton channels in lipid bilayers. Nature. 2010; 463:689–692. [PubMed: 20130653]
23. Pielak RM, Oxenoid K, Chou JJ. Structural investigation of rimantadine inhibition of the AM2-BM2 chimera channel of influenza viruses. Structure. 2011; 19:1655–1663. [PubMed: 22078564]
24. Oxenoid K, Chou JJ. The structure of phospholamban pentamer reveals a channel-like architecture in membranes. Proc Natl Acad Sci U S A. 2005; 102:10870–10875. [PubMed: 16043693]
25. Schnell JR, Chou JJ. Structure and mechanism of the M2 proton channel of influenza A virus. Nature. 2008; 451:591–595. [PubMed: 18235503]
26. Van Horn WD, et al. Solution nuclear magnetic resonance structure of membrane-integral diacylglycerol kinase. Science. 2009; 324:1726–1729. [PubMed: 19556511]
27. Hou X, Pedi L, Diver MM, Long SB. Crystal structure of the calcium release-activated calcium channel Orai. Science. 2012; 338:1308–1313. [PubMed: 23180775]
28. StGelais C, et al. Determinants of hepatitis C virus p7 ion channel function and drug sensitivity identified in vitro. J Virol. 2009; 83:7970–7981. [PubMed: 19493992]
29. Foster TL, et al. Resistance mutations define specific antiviral effects for inhibitors of the hepatitis C virus p7 ion channel. Hepatology. 2011; 54:79–90. [PubMed: 21520195]
30. Cuello LG, Jogini V, Cortes DM, Perozo E. Structural mechanism of C-type inactivation in K(+) channels. Nature. 2010; 466:203–208. [PubMed: 20613835]
31. Schnell JR, Chou JJ. Structure and mechanism of the M2 proton channel of influenza A virus. Nature. 2008; 451:591–595. [PubMed: 18235503]
32. Pielak RM, Oxenoid K, Chou JJ. Structural investigation of rimantadine inhibition of the AM2-BM2 chimera channel of influenza viruses. Structure. 2011; 19:1655–1663. [PubMed: 22078564]
33. Pervushin K, Riek R, Wider G, Wuthrich K. Attenuated T2 relaxation by mutual cancellation of dipole-dipole coupling and chemical shift anisotropy indicates an avenue to NMR structures of very large biological macromolecules in solution. Proc Natl Acad Sci U S A. 1997; 94:12366–12371. [PubMed: 9356455]
34. Kay LE, Torchia DA, Bax A. Backbone dynamics of proteins as studied by 15N inverse detected heteronuclear NMR spectroscopy: application to staphylococcal nuclease. Biochemistry. 1989; 28:8972–8979. [PubMed: 2690953]
35. Szyperski T, Neri D, Leiting B, Otting G, Wuthrich K. Support of 1H NMR assignments in proteins by biosynthetically directed fractional 13C-labeling. J Biomol NMR. 1992; 2:323–334. [PubMed: 1324756]
36. Chou JJ, Gaemers S, Howder B, Louis JM, Bax A. A simple apparatus for generating stretched polyacrylamide gels, yielding uniform alignment of proteins and detergent micelles. J Biomol NMR. 2001; 21:377–382. [PubMed: 11824758]
37. Sass HJ, Musco G, Stahl SJ, Wingfield PT, Grzesiek S. Solution NMR of proteins within polyacrylamide gels: Diffusional properties and residual alignment by mechanical stress or embedding of oriented purple membranes. Journal of Biomolecular Nmr. 2000; 18:303–309. [PubMed: 11200524]

38. Tckyo R, Blanco FJ, Ishii Y. Alignment of biopolymers in strained gels: A new way to create detectable dipole-dipole couplings in high-resolution biomolecular NMR. J Am Chem Soc. 2000; 122:9340–9341.

39. Weigelt J. Single Scan, Sensitivity- and Gradient-Enhanced TROSY for Multidimensional NMR Experiments. J Am Chem Soc. 1998; 120:10778–10779.

40. Wu J, Fan JS, Pascal SM, Yang D. General method for suppression of diagonal peaks in heteronuclear-edited NOESY spectroscopy. J Am Chem Soc. 2004; 126:15018–15019. [PubMed: 15547985]

41. Schwieters CD, Kuszewski J, Tjandra N, Clore GM. The Xplor-NIH NMR molecular structure determination package. J Magn Reson. 2002; 160:66–74.

42. Cornilescu G, Delaglio F, Bax A. Protein backbone angle restraints from searching a database for chemical shift and sequence homology. J Biomol NMR. 1999; 13:289–302. [PubMed: 10212987]

43. Laskowski RA, MacArthur MW, Moss DS, Thornton JW. PROCHECK: a program to check the stereochemical quality of protein structures. J Appl Cryst. 1993; 26:283–291.

44. Plugge B, et al. A potassium channel protein encoded by chlorella virus PBCV-1. Science. 2000; 287:1641–1644. [PubMed: 10698737]

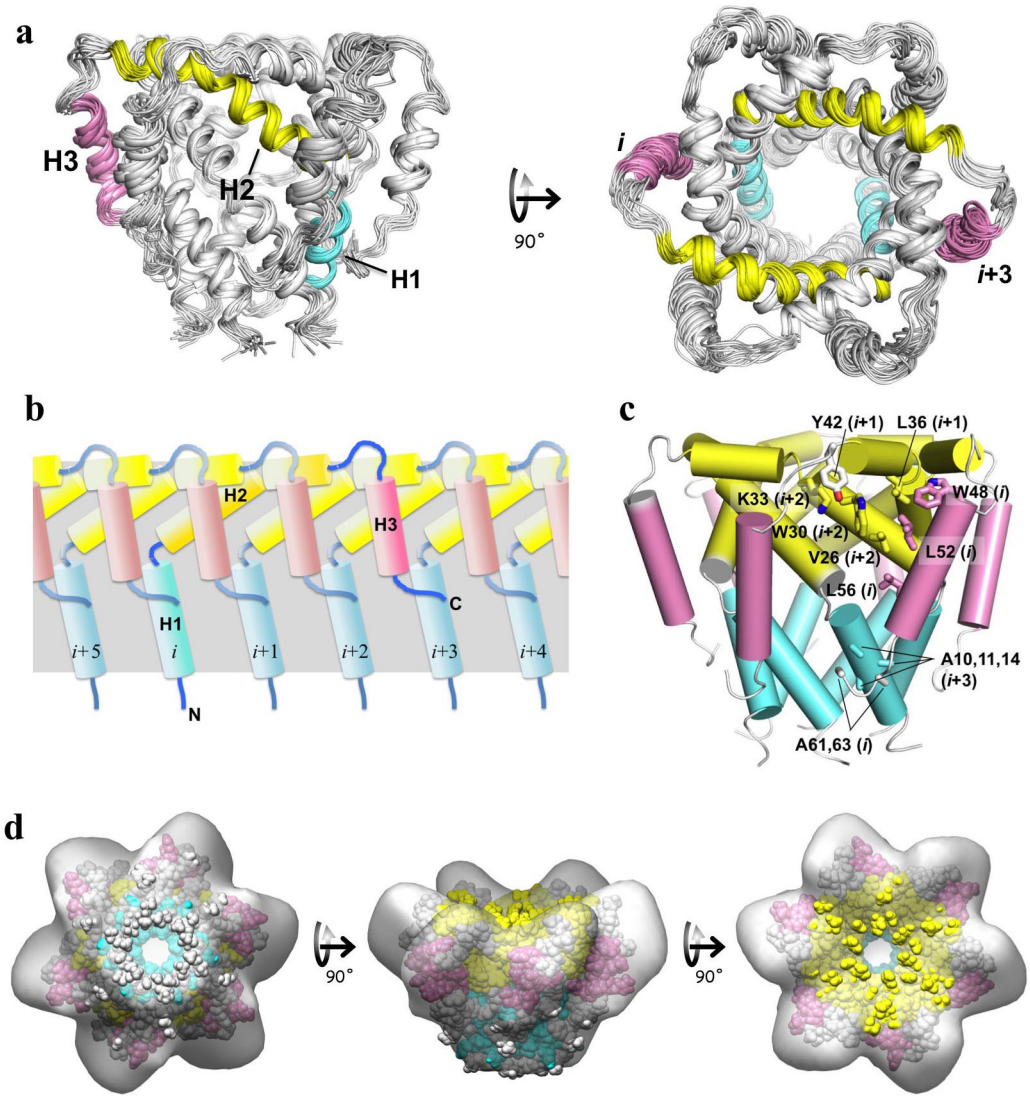

Figure 1. NMR structure of the p7(5a) hexamer and its comparison to the EM map

a, Ensemble of 15 low-energy structures calculated using NMR restraints summarized in Supplementary Table 1. **b**, Two-dimensional drawing illustrating the intermonomer interactions among the H1, H2, and H3 helical segments that are responsible for the hexameric assembly. **c**, Three-dimensional cartoon representation describing the global arrangement of helical segments and amino acids that appear to play a role in the packing of H3 against H1 and H2. **d**, Fitting the lowest energy structure from the ensemble to the 16 Å EM map (EM database ID:1661)[4]. The fitting correlation is 0.94 as calculated with the program Chimera.

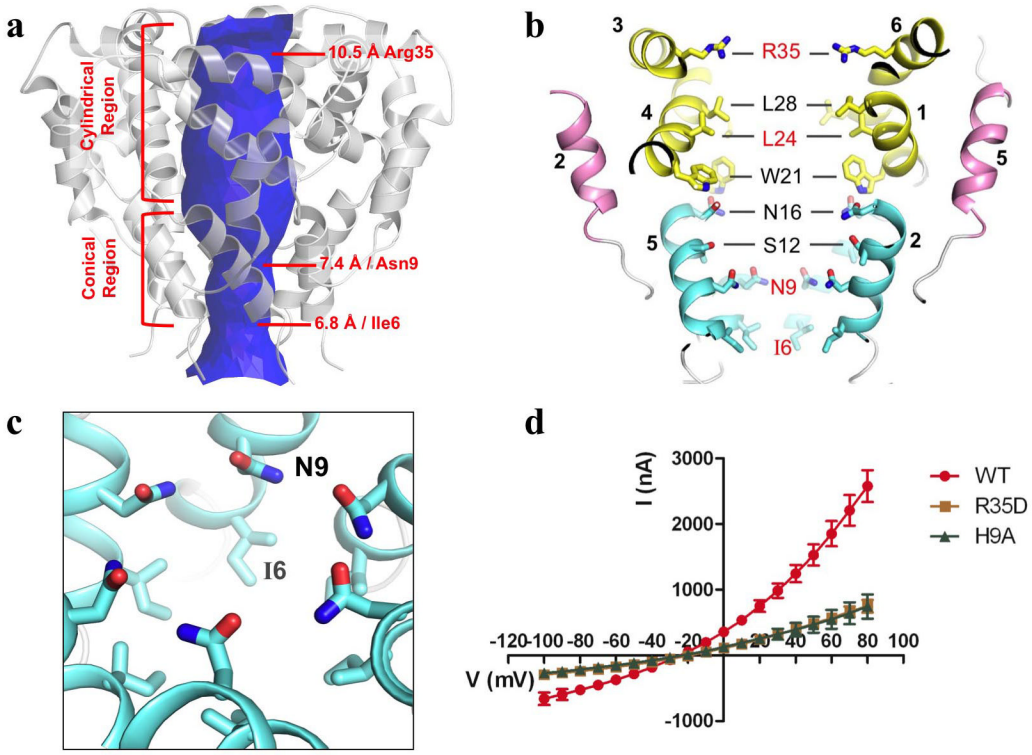

Figure 2. The pore properties of the p7(5a) channel

a, The pore surface calculated using the program HOLE, showing the shape and constrictions of the pore. **b**, Sectional view of the channel showing the pore-lining residues with residues in red being strongly conserved. The numbers next to the helical segments represent the monomers to which the helices belong. **c**, A close view of the rings formed by Asn9 and Ile6 that constrict the N-terminal end of the channel. **d**, The current-voltage relationships of wildtype p7(2a) and the H9A and R35D mutants. Each data point is the mean ± SEM (standard error of mean) calculated over measurements from six different oocytes (n=6).

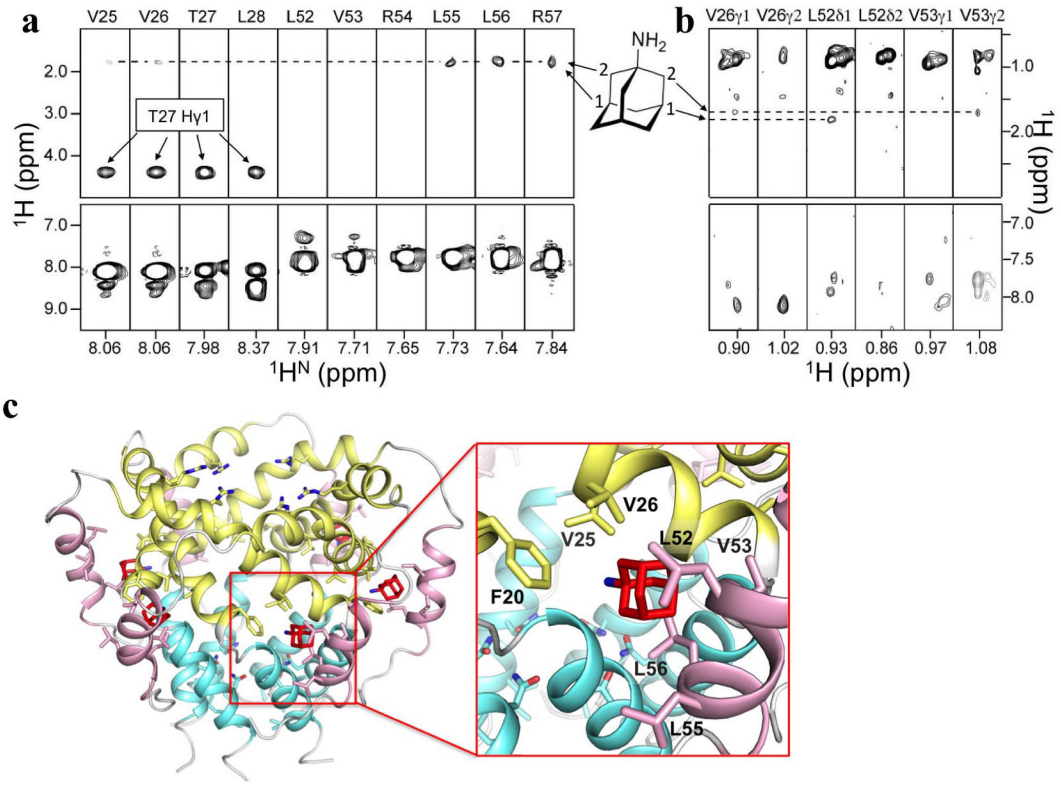

Figure 3. NMR characterization of the amantadine binding site

a, Representative strips from the 3D ^{15}N-edited NOESY-TROSY spectrum (300 ms NOE mixing time) recorded using a sample containing ^{15}N-, ^{2}H-labeled p7(5a) and 10 mM amantadine, showing amantadine NOEs to the backbone amide protons of Val26, Leu55, Leu56, and Arg57. **b**, Representative strips from the 3D diagonal-suppressed ^{13}C-edited NOESY-HSQC spectrum recorded using a sample that is ^{1}H-, ^{13}C-labeled at the methyl positions of alanines, valines and leucines but is otherwise deuterated, showing drug NOEs to the sidechain methyl protons of Val26, Leu52, and Val53. The spectra in **a** and **b** were recorded at ^{1}H frequency of 900 MHz. **c**, Amantadine docked into the p7(5a) hexamer using restraints from NOEs in **a** and **b** (left) and a close view of amantadine in the binding pocket (right).

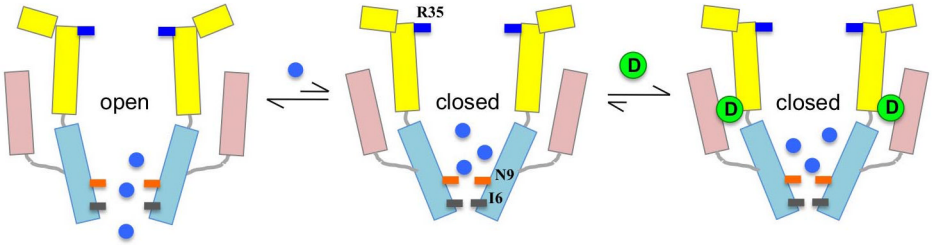

Figure 4. A model for amantadine or rimantadine inhibition of the p7 channel

The two-dimensional cartoon drawing mimics the sectional view of the p7 channel in Fig. 2b. The channel undergoes conformational switching between the closed and the open states but favors the open state in the presence of cations (blue circles). Binding of amantadine or rimantadine (green circle) favors the closed state by restricting movements of the three helical segments that may be required for channel opening.